

# Statistics of Weak Gravitational Lensing in Cold Dark Matter Models; Magnification Bias on Quasar Luminosity Functions

Takashi Hamana,<sup>1</sup> Hugo Martel,<sup>2</sup> and Toshifumi Futamase<sup>1</sup>

## ABSTRACT

We compute statistical properties of weak gravitational lensing by large-scale structure in three Cold Dark Matter (CDM) models: two flat models with  $(\Omega_0, \lambda_0) = (1, 0)$  and  $(0.3, 0.7)$  and one open model with  $(\Omega_0, \lambda_0) = (0.3, 0)$ , where  $\Omega_0$  and  $\lambda_0$  are the density parameter and cosmological constant, respectively. We use a Particle-Particle/Particle-Mesh (P<sup>3</sup>M)  $N$ -body code to simulate the formation and evolution of large-scale structure in the universe. We perform  $1.1 \times 10^7$  ray-tracing experiments for each model, by computing the Jacobian matrix along random lines of sight, using the multiple lens-plane algorithm. From the results of these experiments, we calculate the probability distribution functions of the convergences, shears, and magnifications, and their root-mean-square (rms) values. We find that the rms values of the convergence and shear agree with the predictions of a nonlinear analytical model. We also find that the probability distribution functions of the magnifications  $\mu$  have a peak at values slightly smaller than  $\mu = 1$ , and are strongly skewed toward large magnifications. In particular, for the high-density ( $\Omega_0 = 1$ ) model, a power-law tail appears in the distribution function at large magnifications for sources at redshifts  $z_s > 2$ . The rms values of the magnifications essentially agree with the nonlinear analytical predictions for sources at low redshift, but exceed these predictions for high redshift sources, once the power-law tail appears.

We study the effect of magnification bias on the luminosity functions of high-redshift quasars, using the calculated probability distribution functions of the magnifications. We show that the magnification bias is moderate in the absence of the power-law tail in the magnification distribution, but depends strongly on the value of the density parameter  $\Omega_0$ . In presence of the power-law tail, the bias becomes considerable, especially at the bright end of the luminosity functions where its logarithmic slope steepens. We present a specific example which demonstrates that the bias flattens the bright side logarithmic slope of a double power-law luminosity function.

*Subject headings:* cosmology: observations — cosmology: theory — gravitational lensing — large-scale structure of universe — quasars: general

## 1. INTRODUCTION

It is well known that the apparent brightness of distant sources are gravitationally affected by the inhomogeneous distribution of matter in the universe, an effect called the lensing magnification. Consequently, the apparent brightness and intrinsic luminosity of a distant source are no longer simply

---

<sup>1</sup>Astronomical Institute, Tohoku University, Sendai 980-8578, Japan

<sup>2</sup>Department of Astronomy, University of Texas, Austin, TX 78712

related by the luminosity distance-redshift relation in a smooth Friedmann universe (Weinberg 1972; Schneider, Ehlers, & Falco 1992, hereafter SEF). The relation depends on how light rays are being lensed by density inhomogeneities in the universe, as they propagate from the source to the observer. Since the pioneering works of Kristian & Sachs (1966) and Gunn (1967), numerous studies of the effect of lensing magnification in an inhomogeneous universe have been published. Two different approaches have been used in these studies to compute the statistical properties of lensing magnifications in inhomogeneous universes with realistic matter distributions: the power spectrum approach, which is analytical, and the numerical approach, which combines  $N$ -body simulations of structure formation with ray-tracing simulations.

The power spectrum approach was first developed by Gunn (1967), who showed that the root-mean-square (rms) fluctuation in the apparent brightness of distant sources (or equivalently in the lensing magnification) can be expressed as a radial integral of the density autocorrelation function. Gunn’s original approach was eventually modified by Babul & Lee (1991) to reflect substantial advances in our understanding of large-scale structure formation. These authors gave a quantitative estimate of the rms fluctuations for modern cosmological models such as the Cold Dark Matter (CDM) model. Frieman (1997) rederived the rms fluctuations using the Limber’s equation in Fourier space (Kaiser 1992, 1998), and found that the dispersion in the lensing magnification can be larger than 0.1 for sources at redshift  $z_s = 1$ , but depends strongly on the background cosmological model. The skewness of the probability distribution of the lensing magnifications was first calculated by Nakamura (1997) using the quasi-linear theory of density fluctuation.

The first study based on the numerical approach was done by Jaroszyński et al. (1990), who used a Particle-Mesh (PM)  $N$ -body code to simulate the formation and evolution of large-scale structure in a CDM universe. The multiple lens-plane algorithm developed by Blandford & Narayan (1986) and Kovner (1987) was then used to follow the evolution of ray bundles propagating through the inhomogeneous matter distribution in the simulated universes. The force resolution of the PM simulations was  $1h^{-1}\text{Mpc}$ , in present units (where  $h$  is the Hubble constant  $H_0$  in units of  $100\text{ km s}^{-1}\text{Mpc}^{-1}$ ), not sufficient to include lensing effects by small-scale nonlinear structures like galaxy clusters. They found that the rms values of the lensing magnifications by large-scale structure are very small even for sources at redshift  $z_s = 5$ . Since then, this method has been improved by several authors (Bartelmann & Schneider 1991, 1992; Jaroszyński 1991, 1992; Wambsganss et al. 1995, 1997; Wambsganss, Cen & Ostriker 1998; Premadi, Martel & Matzner 1998; Tomita 1998a, 1998b). Thanks to their effort and recent rapid developments of computational techniques as well as computing power, the length resolution of these algorithms has significantly improved. For instance, Wambsganss et al. (1998) used large PM  $N$ -body simulations combined with a convolution method and have achieved an effective resolution of  $10h^{-1}\text{kpc}$ .

Jaroszyński (1991, 1992) extended the length resolution of the method to subgalactic scales by combining numerical simulations of large-scale structure formation with a Monte-Carlo method for locating galaxies inside the computational volume. Galaxies were modeled as isothermal spheres with velocity dispersions and core radii determined by empirical relations depending on morphological types. Ray-tracing simulations were then performed, taking into account the combined effects of the large-scale structure and the galaxies. Later, Premadi et al. (1998) improved this method significantly, first by replacing the Zel’dovich algorithm used by Jaroszyński for simulating large-scale structure formation by a more accurate Particle-Particle/Particle-Mesh ( $P^3M$ )  $N$ -body code, and then by taking into account, when assigning morphological types to galaxies, the observed morphology-density relation (Martel, Premadi, & Matzner 1998 and references therein).

In this paper, we use the multiple lens-plane algorithm to study the effect of lensing by large-scale

structure on quasar luminosity functions. We focus on CDM models with a *COBE*-normalized tilted power spectrum (Bunn & White 1997). The P<sup>3</sup>M simulations for these models were provided by the Texas P<sup>3</sup>M Database (Martel & Matzner 1999). Each model is characterized by the value of 4 parameters: the density parameter  $\Omega_0$ , cosmological constant  $\lambda_0$ , Hubble constant  $H_0$ , and rms density fluctuation  $\sigma_8$  at scale  $8h^{-1}\text{Mpc}$  (the tilt  $n$  of the power spectrum is a dependent parameter). We consider three particular models, an Einstein de Sitter model (E-dS) with  $\Omega_0 = 1$  and  $\lambda_0 = 0$ , an open model (O) with  $\Omega_0 = 0.3$  and  $\lambda_0 = 0$ , and a flat model ( $\Lambda$ ) with  $\Omega_0 = 0.3$  and  $\lambda_0 = 0.7$ . For each model, we follow the propagation of light ray bundles through the matter distribution. We are primarily interested in the statistical properties of lensing by the matter inhomogeneities in the universe, and not in rare events such as multiple imaging of distant quasars. Consequently, we focus on the lensing effects by the large-scale ( $> 0.1h^{-1}\text{Mpc}$ ) structures and make no attempt to study lensing effects caused by individual galaxies.

In order to obtain good statistics, we perform a total of  $1.1 \times 10^7$  ray-tracing experiments for each model. Each experiment consists of computing the Jacobian matrix along a random line of sight. Having such a large number of experiments allows us to study in detail not only rms values, but also the probability distribution functions of the lensing properties, i.e., the convergence, shear, and magnification. We compare these rms values with predictions based on the power spectrum approach. This enables us to test the validity of the power spectrum approach and its limitation.

Using the probability distribution functions of the lensing magnifications obtained from the experiments, we study the effects of the magnification bias on quasar luminosity functions. This problem was first studied by Sanitt (1971), and later by many different authors (e.g., Turner 1980; Avni 1981; Canizares 1982; Peacock 1982; Vietri 1985; Ostriker & Vietri 1986; Schneider 1987b, 1987c, 1992; see also SEF, chapter 12). A crucial difference between these previous studies and ours is that we compute the probability distribution in universes with realistic matter distributions, that originate from the growth of primordial density fluctuations with a specific power spectrum and normalization, and are simulated using a state-of-the-art  $N$ -body code. In previous studies, the probability distribution was calculated by considering simple matter distributions such as randomly distributed point masses and/or isothermal spheres. These studies revealed that the magnification bias can have a considerable effect on the luminosity functions, especially for bright quasars (Ostriker & Vietri 1986; Schneider 1992). However, they cannot be used to make predictions about the effect on the magnification bias in specific cosmological models, since this requires a realistic representation of the large-scale structure in the universe.

We demonstrate the importance of the bias on quasar luminosity functions and show its dependence on the mean matter density of the universe. However, we do not attempt to derive a precise quantitative estimate of the bias on the observed luminosity functions. This would require a precise knowledge of both the observed luminosity functions and the probability distribution of the lensing magnifications. However, uncertainties in the quasar luminosity functions are still considerable (e.g., Boyle, Shanks, & Peterson 1988; Hartwick & Schade 1990; Warren, Hewett, & Osmer 1994; Hawkins & Véron 1995; La Franca & Cristiani 1997). Furthermore, the magnification distributions we calculate are those for a point like source, the effect of finite source size on the magnification probability becomes important at large magnifications (Schneider 1987b; Schneider & Weiss 1988a, 1988b). Because of these limitations, we decided to approximate the intrinsic quasar luminosity functions using either a single or a double power-law model. Although it is not clear whether the power-law models provide an accurate description of a real luminosity function, we believe that these models are sufficiently realistic (especially the double power-law model) for a qualitative study of the essential properties of the magnification bias.

The remainder of this paper is organized as follows: In §2, we describe the cosmological models, and the

numerical methods used for simulating both the large-scale structure formation and the light propagation. In §3, we present the results of the experiments and compared them with predictions based on the power spectrum approach. In §4, we discuss the effects of magnification bias on the quasar luminosity functions. Summary and conclusion are presented in §5. In Appendix A, we summarize the basic equations used in the power spectrum approach.

## 2. DESCRIPTIONS OF THE COSMOLOGICAL MODELS AND NUMERICAL METHODS

### 2.1. Cold Dark Matter Models

We consider three tilted CDM cosmological models. Each model is characterized by its values of  $\Omega_0$ ,  $\lambda_0$ ,  $H_0$ , and  $\sigma_8$ , with the primordial exponent  $n$  being a dependent parameter (Martel & Matzner 1999; Premadi et al. 1999). Table 1 lists the models and gives their parameters. The power spectrum is given by

$$P(k) = 2\pi^2 \left( \frac{c}{H_0} \right)^{3+n} \delta_H^2 k^n T^2(k), \quad (1)$$

where  $c$  is the speed of light. The transfer function  $T(k)$  for CDM models is given by Bardeen et al. (1986) as follows,

$$T(q) = \frac{\ln(1 + 2.34q)}{2.34q} [1 + 3.89q + (16.1q)^2 + (5.46q)^3 + (6.71q)^4]^{-1/4}, \quad (2)$$

where  $q$  is defined by

$$q = \left( \frac{k}{\text{Mpc}^{-1}} \right) \alpha^{-1/2} (\Omega_0 h^2)^{-1} \Theta_{2.7}^2, \quad (3)$$

$$\alpha = a_1^{-\Omega_{B0}/\Omega_0} a_2^{-(\Omega_{B0}/\Omega_0)^3}, \quad (4)$$

$$a_1 = (46.9\Omega_0 h^2)^{0.670} [1 + (32.1\Omega_0 h^2)^{-0.532}], \quad (5)$$

$$a_2 = (12.0\Omega_0 h^2)^{0.424} [1 + (45.0\Omega_0 h^2)^{-0.582}], \quad (6)$$

(Hu & Sugiyama 1996), where  $\Theta_{2.7}$  is the cosmic microwave background temperature in units of 2.7K, and  $\Omega_{B0}$  is the contribution of baryons to the density parameter. In all models,  $\Theta_{2.7}$  and  $\Omega_{B0}$  were set equal to 1 and  $0.015h^{-2}$  respectively. The density perturbation  $\delta_H$  at horizon crossing is obtained by fitting the

Table 1. Summary of model parameters

Model	$\Omega_0$	$\lambda_0$	$\Omega_{B0}h^2$	$h$	$\sigma_8$	$n$
E-dS	1.0	0.0	0.015	0.65	1.20	0.8506
O	0.3	0.0	0.015	0.75	0.85	1.1748
$\Lambda$	0.3	0.7	0.015	0.75	0.90	0.8796

COBE 4-year data (Bunn & White 1997), as follows,

$$10^5 \delta_H = \begin{cases} 1.95 \Omega_0^{-0.35-0.19 \ln \Omega_0 - 0.17 \tilde{n}} e^{-(\tilde{n}+0.14 \tilde{n}^2)}, & \lambda_0 = 0; \\ 1.94 \Omega_0^{-0.785-0.05 \ln \Omega_0} e^{-(0.95 \tilde{n}+0.169 \tilde{n}^2)}, & \lambda_0 = 1 - \Omega_0; \end{cases} \quad (7)$$

where  $\tilde{n} \equiv n - 1$ .

## 2.2. The P<sup>3</sup>M Algorithm

The simulations of large-scale structure formation were provided by the Texas P<sup>3</sup>M Database (Martel & Matzner 1999). All simulations were performed using a P<sup>3</sup>M  $N$ -body code (Hockney & Eastwood 1988) with  $64^3$  particles, in a computational cubic box with triply periodic boundary conditions. The forces on particles are computed by solving Poisson’s equation on a  $128^3$  cubic lattice using a Fast Fourier Transform method. The forces at short distance are corrected by direct summation over pairs of particles separated by less than some cutoff distance  $r_e$  equal to a few grid spacings. The algorithm reproduces accurately the Newtonian interaction between particle down to the softening length  $\eta$ , which is set equal to a fraction of the grid spacing. In all simulations, the comoving lengths of the size  $L_{\text{box}}$  of the computational box and the softening length  $\eta$  were equal to 128 Mpc and 300 kpc, respectively. Hence, the algorithm has a dynamical range of 427 in length. Notice that in this paper, we express distances in units of  $h^{-1}$  Mpc. In these units, the values of  $L_{\text{box}}$  and  $\eta$  vary among models. These values, and also the mass per particle, are listed in Table 2. Three simulations were performed for each cosmological model. For each model, the simulations differ only in the choice of random phases in the initial conditions. All simulations start at an initial redshift of  $z = 24$ , and end at  $z = 0$ .

We calculated the two-point correlation function of the particles at redshifts  $z = 0$ ,  $z = 1$ , and  $z = 2$  using a direct estimator (Hockney & Eastwood 1988),

$$\xi(r) = \frac{N_p}{\bar{n} N_c \delta V} - 1, \quad (8)$$

where  $N_p$  is the number of particles inside a spherical shell of inner radius  $r - \Delta r/2$  and outer radius  $r + \Delta r/2$  centered around a central particle,  $\delta V$  is the volume of this shell,  $N_c$  is the number of particles taken as centers, and  $\bar{n}$  is the mean number density of the particles. The results are plotted in Figure 1. For comparison, we plot analytical estimates of the two-point correlation function, based both on linear perturbation theory and on the nonlinear power spectrum fitting formula of Peacock & Dodds (1996), and

Table 2. Parameters in P<sup>3</sup>M simulations

Model	Box Size, $L_{\text{box}}$ ( $h^{-1}$ Mpc)	Particle mass ( $h^{-1}M_{\odot}$ )	Softening length, $\eta$ ( $h^{-1}$ Mpc)
E-dS	83.2	$3.608 \times 10^{11}$	0.195
O and $\Lambda$	96.0	$1.249 \times 10^{11}$	0.225

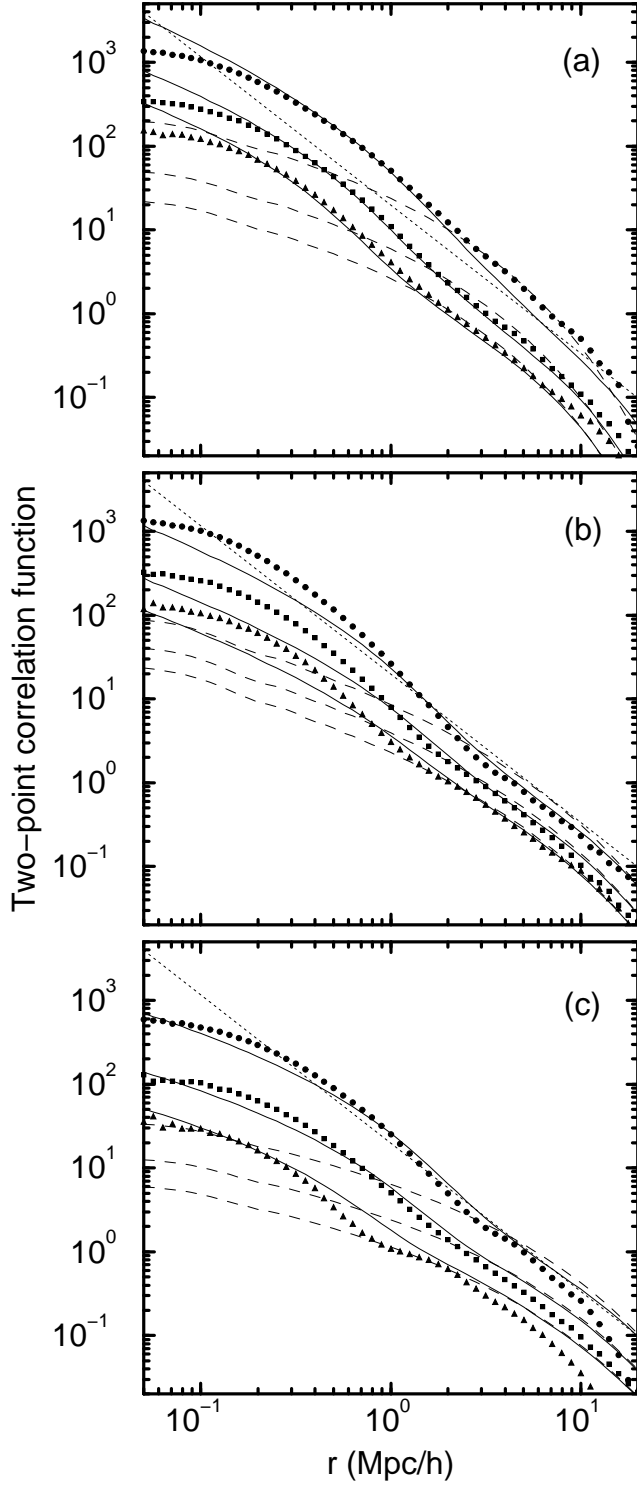


Fig. 1.— Two-point correlation functions compared with those predicted by the linear theory and (a) is for E-dS model, (b) is for O model and (c) is for  $\Lambda$  model. The filled symbols represent the two-point correlation functions calculated from the particle positions in the P<sup>3</sup>M simulations. Filled circles, squares, and triangles corresponds to redshifts  $z = 0$ ,  $z = 1$ , and  $z = 2$ , respectively. Solid lines show the correlation function derived from the non-linear power spectrum, using the fitting formula by Peacock & Dodds (1996). Dashed lines show the correlation functions predicted by linear theory. The redshifts are  $z = 0$ , 1 and 2 from top to bottom, respectively. The dotted line shows the observed galaxy two-point correlation function.

also the observed galaxy 2-point correlation function at the present epoch,

$$\xi(r) = \left( \frac{r}{5.4 h^{-1} \text{Mpc}} \right)^{-1.77} \quad (9)$$

(Peebles 1993). As we see in Figure 1 the slope the correlation functions drop significantly at short range, for  $r < \eta$ . Martel (1991) pointed out that this flattening of  $\xi$  is due to the softening of the force, which reduces the number of particle pairs with separations  $r \lesssim \eta$ , and increases the number of pairs with separations  $r \gtrsim \eta$ . For the E-dS model, the correlation functions obtained from the P<sup>3</sup>M simulation are in good agreement with the nonlinear predictions. For the O and  $\Lambda$  models, the nonlinear predictions are slightly smaller than the correlation functions obtained from the simulations at intermediate pair separations ( $\eta < r < 1h^{-1}\text{Mpc}$ ). In §2.3, we examine the statistical properties of the gravitational lensing by these simulated matter distributions, and compare the rms values of the lensing convergences, shears, and magnifications with the predictions of the power spectrum approach using Peacock & Dodds’ fitting formula for the nonlinear power spectrum. Therefore, the reader should keep in mind that, for the O and  $\Lambda$  models, Peacock & Dodds’ fitting formula slightly underestimates the correlation function at short range,  $r < 1h^{-1}\text{Mpc}$ , and thus we can expect that the rms values of the convergences, shears, and magnifications predicted by the power spectrum approach will be also underestimated.

### 2.3. The Ray-Tracing Experiments

We use the multiple-lens plane algorithm to follow the evolution of light rays traveling through the simulated matter distributions. The P<sup>3</sup>M simulations provided particle distributions in cubic boxes at various redshifts, from the initial redshift  $z = 24$  to to present. By combining these boxes, we can represent the matter distribution in the universe along a line of sight extending from the observer to the source.<sup>3</sup> For sources at redshift  $z_s = 3$ , this requires 36 boxes for the E-dS model, 38 for the O model, and 47 for the  $\Lambda$  model. In order to eliminate spurious correlations between the large-scale structure in adjacent boxes, we combine boxes from different simulations, so that cubic boxes which are directly joined to each other are chosen from different simulations.

In the standard multiple-lens plane algorithm, the matter content of each box is projected onto a single plane perpendicular to the line of sight. We increase the accuracy of the algorithm by dividing the cubic box into four rectangular subboxes of size  $L_{\text{box}} \times L_{\text{box}} \times (L_{\text{box}}/4)$ , and projecting the matter content of each subbox onto a plane, thus increasing the number of lens planes by a factor of 4.

The deflection potential  $\psi^i$  on the  $i$ -th lens plane is related to the surface mass density fluctuation  $\delta\Sigma_i(\vec{x}) = \Sigma_i(\vec{x}) - \langle \Sigma_i \rangle$  on that plane by

$$\psi^i(\vec{x}) = \frac{1}{\pi} \iint d^2x' \delta\Sigma_i(\vec{x}') \ln \frac{|\vec{x} - \vec{x}'|}{x_0}, \quad (10)$$

where  $\vec{x} = (x_1, x_2)$  is the position vector in the plane, and  $x_0$  is an arbitrary cutoff length (its value is irrelevant, since only derivatives of  $\phi^i$  have a physical signification). This equation can be rewritten in the

---

<sup>3</sup>This approach ignores the possible existence of structures larger than  $L_{\text{box}} = 128 \text{Mpc}$ . This does not effect on our experiments in any significant way, because in the CDM universe, fluctuations at that scale have a very small amplitude even at the present time, and their lensing effect is negligibly small.

form of a two-dimensional Poisson equation,

$$\nabla^2 \psi^i = 2\delta\Sigma_i. \quad (11)$$

We solve this equation numerically on each lens plane by first computing the surface density on a  $512 \times 512$  square lattice from the particle positions, using the Triangular Shaped Cloud (TSC) assignment scheme (Hockney & Eastwood 1988, §5.3), and then inverting equation (11) using a Fast Fourier Transform method (see, e.g., Premadi et al. 1998). Notice that the grid spacings are  $0.1625h^{-1}\text{Mpc}$  for the E-dS model and  $0.1875h^{-1}\text{Mpc}$  for the O and  $\Lambda$  models, and are slightly smaller than the softening length  $\eta$  of the P<sup>3</sup>M calculations. The evolution equation of the Jacobian matrix in the multiple-lens plane algorithm is given by

$$\mathbf{A}_{j+1} = \mathbf{I} - \frac{4\pi G}{c^2} \sum_{i=1}^j \frac{D_i D_{ij}}{D_j} \mathbf{U}_i \mathbf{A}_i, \quad (12)$$

where  $D_j$  is the angular diameter distance between the observer and the  $j$ -th lens plane,  $D_{ij}$  is the angular diameter distance between the  $i$ -th,  $j$ -th lens plane, and  $\mathbf{U}_i$  is an optical tidal matrix defined by,

$$\mathbf{U}_i = \begin{pmatrix} \psi_{,11}^i & \psi_{,12}^i \\ \psi_{,12}^i & \psi_{,22}^i \end{pmatrix} = \begin{pmatrix} \delta\Sigma_i + \frac{1}{2}(\psi_{,11}^i - \psi_{,22}^i) & \psi_{,12}^i \\ \psi_{,12}^i & \delta\Sigma_i - \frac{1}{2}(\psi_{,11}^i - \psi_{,22}^i) \end{pmatrix}, \quad (13)$$

with commas denoting differentiation with respect to  $\vec{x}$ . The last equality was obtained using equation (11). We compute the second derivatives of  $\psi^i$  on grid points using a standard finite difference formula.

In general, equation (12) is not an explicit equation for  $\mathbf{A}_i$  since the summation contains the tidal matrix  $\mathbf{U}_i$ , which must be evaluated along the light ray path. One first has to solve the multiple gravitational lens equation in order to compute the location of the light ray on each lens plane and then evaluate  $\mathbf{U}_i$  at that location. However, the deflections of light rays are very small; the deflection angle caused by structures larger than  $0.1h^{-1}\text{Mpc}$  is at most  $\alpha \sim 10^{-5}$ . The distance between the actual and unperturbed positions of a light ray will be much smaller than the grid spacing of the lattice used for calculating the two-dimensional potential and its derivatives. To give an actual example, the transverse distance from the unperturbed ray position is at most  $l_{\perp} \sim L_{\text{box}}\alpha < 10^{-3}h^{-1}\text{Mpc}$  for a light ray propagating a comoving distance of  $L_{\text{box}}$ . We can therefore treat light rays as if they were moving along straight lines.<sup>4</sup> This greatly simplifies the algorithm. Not only the computation of light ray trajectories becomes unnecessary, but in addition we can choose lines of sights that go through the grid points, where the surface mass density fluctuation  $\delta\Sigma_i$  and the derivatives  $\psi_{,11}^i$ ,  $\psi_{,22}^i$  and  $\psi_{,12}^i$  of the potential are known, thus eliminating the need to interpolate  $\mathbf{U}_i$  from the grid points to the location of the rays. Since the lattice is composed of  $512 \times 512 = 262\,144$  grid points, there are 262 144 possible lines of sight to choose from. Each experiments consists of selecting one line of sight, and solving equation (12) recursively along that line of sight for all values of  $\mathbf{A}_j$ , starting with  $\mathbf{A}_1 = \mathbf{I}$  (the identity matrix). It may seem that the number of possible experiments is limited to 262 144, but actually, since the P<sup>3</sup>M simulations use periodic boundary conditions, each cubic box can be given a random shift, or, equivalently, any grid point in a cubic box can be chosen, independently of the ones chosen in other cubic boxes, as long as the same grid point is chosen on the four lens planes within each

---

<sup>4</sup>We could not make this simplification if we were interested in the deformation and/or multiple imaging of sources with a finite size. In that case, it is the relative difference between the deflection angles of nearby rays that matters, and those can be quite large.



box. The total number of possible experiments is therefore  $262\,144^{N_{\text{box}}}$ , where  $N_{\text{box}}$  is the number of cubic boxes along the line of sight.

We decompose the Jacobian matrix as

$$\mathbf{A} = \begin{pmatrix} 1 - \delta\kappa - \gamma_1 & -\gamma_2 - \omega \\ -\gamma_2 + \omega & 1 - \delta\kappa + \gamma_1 \end{pmatrix}, \quad (14)$$

where  $\delta\kappa$  represents a fluctuation of convergence from that in smooth Friedmann universe,  $|\gamma| = (\gamma_1^2 + \gamma_2^2)^{1/2}$  is the amplitude of shear of a light ray bundle, and  $\omega$  is the rotation angle of the beam. The image magnification factor of a point like source is given by the inverse of the determinant of the Jacobian matrix,

$$\mu = \frac{1}{|\det \mathbf{A}|} = \frac{1}{|(1 - \delta\kappa)^2 - \gamma^2 - \omega^2|}. \quad (15)$$

### 3. RESULTS

#### 3.1. Lensing Convergence and Shear

We first study the statistical properties of the lensing convergence  $\delta\kappa$  and shear  $\gamma$ . For this purpose we perform  $10^6$  experiments for each model. The probability distributions of  $\delta\kappa$  and  $\gamma$  are shown in Figure 2 and 3, respectively, for sources at redshifts  $z_s = 1, 2, \text{ and } 3$ . The probability distributions of both  $\delta\kappa$  and  $\gamma$  broaden when the source redshift increases, and those in the E-dS model (top panel) are considerably broad compared with those in the O (middle panel) and  $\Lambda$  (bottom panel) models. The probability distributions are slightly broader in the  $\Lambda$  model than in the O model. These properties are consistent with analytical predictions, as we will demonstrate below. The probability distributions of  $\delta\kappa$  have a peak at some negative value, and are skewed toward positive values. This behavior is prominent in the E-dS model. These distributions are a reflection of the mass distribution in the universe: in most of the universe, the matter density is smaller than the average value, while most of the matter is concentrated into compact structures such as galaxies and clusters of galaxies. Thus, for the majority of the random lines of sight, light ray bundles converge less compared to those propagating through a smooth Friedmann universe. The average values of the fluctuations of the lensing convergence in our simulations are found to be consistent with zero, i.e.,  $|\langle \delta\kappa \rangle| < 10^{-4}$ . There is a minimum value of the fluctuation of the lensing convergence, which occurs when the beam propagates through empty space. It is given by

$$\delta\kappa_{\text{min}} = 1 - \frac{D_{DR}(z)}{D_F(z)}, \quad (16)$$

(SEF, chapter 11; Hamana 1998), where  $D_{DR}(z)$  is the so-called Dyer-Roeder distance (Dyer & Roeder 1972, 1973) with the clumpiness parameter  $\tilde{\alpha} = 0$  (Fukugita et al. 1992), and  $D_F(z)$  is the standard angular diameter distance. The values of  $\delta\kappa_{\text{min}}$  are given in Table 3 for the three cosmological models considered in this paper. Comparing the lower cutoff of the probability distributions found in Figure 2 with these minimum values, we find that a value of  $\delta\kappa$  near  $\delta\kappa_{\text{min}}$  is unlikely to occur in our ray-tracing experiments, especially for sources at a high redshift. This is consistent with the results of Futamase & Sasaki (1989), which are based on a simple analytical approach.

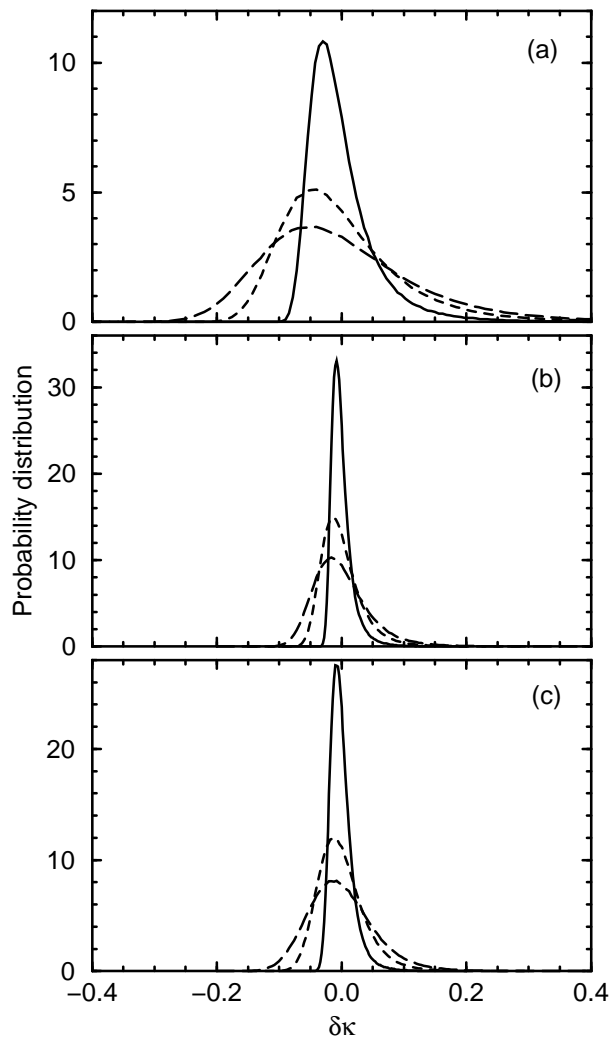


Fig. 2.— Probability distributions of fluctuations of lensing convergence,  $\delta\kappa$ . The solid lines, short-dashed lines, and long-dashed lines correspond to sources at redshifts  $z_s = 1, 2,$  and  $3,$  respectively. (a) E-dS model; (b) O model; (c)  $\Lambda$  model.

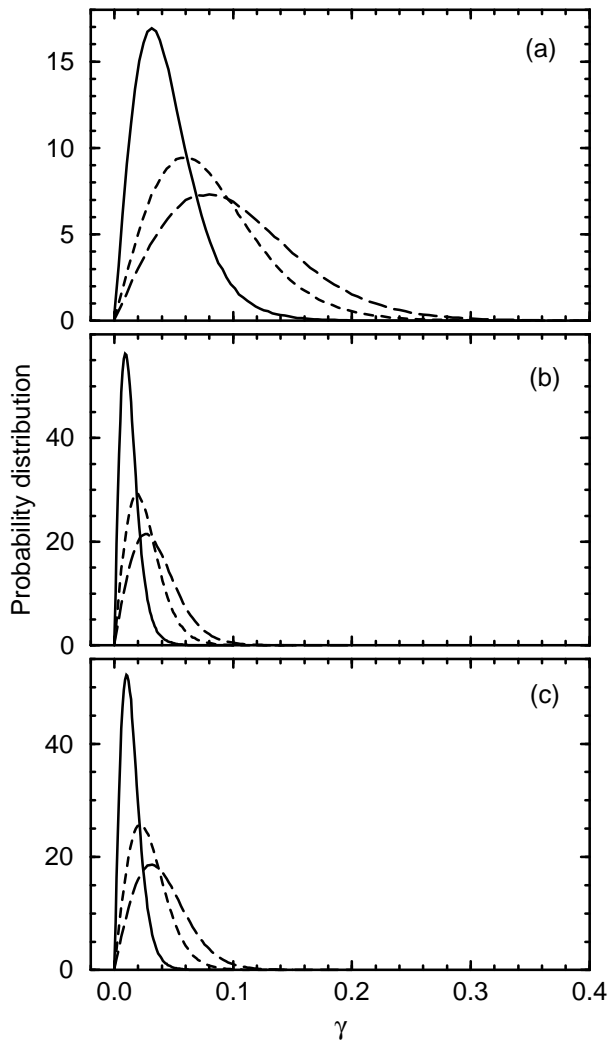


Fig. 3.— Probability distributions of the lensing shear of images. Lines have the same meaning as in Figure 2. (a) E-dS model; (b) O model; (c)  $\Lambda$  model.

In Figure 4, we plot the rms values  $\sigma_\kappa$  of the convergence and  $\sigma_\gamma$  of the shear, defined by

$$\sigma_\kappa = \left[ \frac{1}{N_{\text{exp}}} \sum_{i=1}^{N_{\text{exp}}} (\delta\kappa_i)^2 \right]^{1/2}, \quad (17)$$

$$\sigma_\gamma = \left[ \frac{1}{N_{\text{exp}}} \sum_{i=1}^{N_{\text{exp}}} |\gamma_i|^2 \right]^{1/2}, \quad (18)$$

where  $N_{\text{exp}}$  is the number of experiments. Notice that  $\sigma_\kappa$  and  $\sigma_\gamma$  are expected to be equal, based on analytical arguments (Jain & Seljak 1997). Instead, we find that the rms values of the shear computed from our ray-tracing experiments are slightly but systematically smaller than those of the convergence. However, this difference is probably insignificant, because the shear computed from the experiments might be underestimated, whereas the convergence is probably accurate. The shear is mainly caused by the traceless symmetric part (Weyl part) of the optical tidal matrix  $\mathbf{U}_i$ , which depends upon second derivatives of the two-dimensional potential  $\psi^i$ . These second derivatives can be underestimated somewhat because of the finite resolution of the lattice used for solving equation (11). The lensing convergence is mainly caused by the surface mass density fluctuation  $\delta\Sigma_i$ , which is directly computed from the particle positions.

In each panel of Figure 4, we also plotted three curves, which represent various analytical estimates of  $\sigma_\kappa$  and  $\sigma_\gamma$  (see Appendix A); the solid curves represent predictions based on the power spectrum approach (Kaiser 1992; Bernardeau, van Waerbeke & Mellier 1997; Jain & Seljak 1997; Nakamura 1997), using the nonlinear power spectrum by Peacock & Dodds (1996) (hereafter, we refer to this as the nonlinear method), dashed curves represent the predictions obtained from a top-hat filtered density field with a smoothing scale of  $R_s = 0.1h^{-1}\text{Mpc}$  (the filtered nonlinear method), comparable to the softening length of the P<sup>3</sup>M simulations, and long-dashed curves represent the predictions of linear perturbation theory (the linear method).

The nonlinear method predicts that the rms values scale approximately as  $\sigma_\kappa, \sigma_\gamma \propto \sigma_8 \Omega_0^{0.7-0.8}$  at a fixed source redshift, and increase with the cosmological constant because of the resulting increase in the path length (Bernardeau et al. 1997; Jain & Seljak 1997). In all models, the rms values obtained from our ray-tracing experiments are significantly larger than the predictions of the linear method. These rms values should be compared preferentially to the predictions of the filtered nonlinear method, because the effect of lensing by structures smaller scale than the softening length is not included in our experiments. The rms values obtained from our experiments are slightly smaller than those predicted by the filtered nonlinear method for the E-dS model, and slightly larger for the O and  $\Lambda$  models. It is important to recall that the

Table 3. The minimum values of the fluctuation of the lensing convergence,  $\delta\kappa_{\text{min}}$

Redshift of source $z_s$	E-dS	O	$\Lambda$
1.0	-0.1243	-0.04504	-0.06567
2.0	-0.3285	-0.1274	-0.2071
3.0	-0.5500	-0.2203	-0.3724

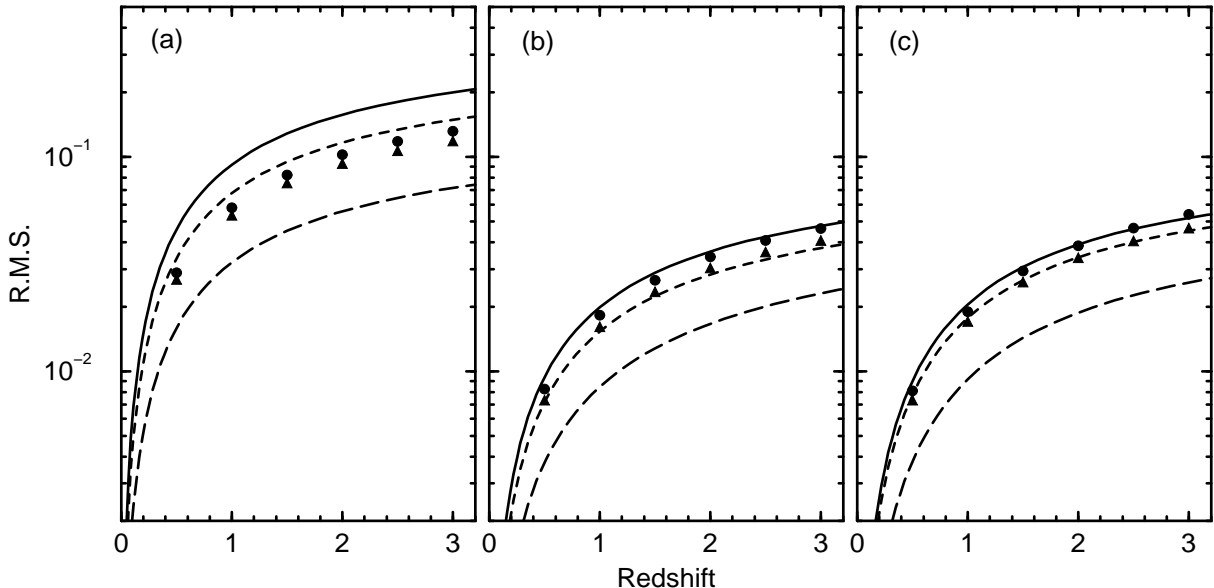


Fig. 4.— Root-mean-squares of the lensing convergence and shear of images as a function of redshifts of source. The filled circles and filled triangle are for the lensing convergence and shear of images evaluated from the results of ray-tracing experiments, respectively. The solid curves represent predictions of the power spectrum approach with the nonlinear power spectrum by Peacock & Dodds (1996), dashed curves are those obtained from a top-hatted density field with a smoothing scale of  $R_s = 0.1h^{-1}\text{Mpc}$ , and long-dashed curves are the predictions of linear perturbation theory. (a) E-dS model; (b) O model; (c)  $\Lambda$  model.

same trends were shown in the two-point correlation functions of the matter (Figure 1). These two trends are consistent with each others at least qualitatively; the correlation function and the rms values are either both overestimated or both underestimated by the nonlinear predictions, depending upon the cosmological model. This suggests that the rms values obtained from our experiments are consistent at least qualitatively with the predictions of the filtered nonlinear method.

These various comparisons show that rms values of the lensing convergence and shear are identical within the uncertainties inherent to the numerical method. They also show that the power spectrum approach with the nonlinear power spectrum provides good estimates for the rms values of the lensing convergences and shears.

### 3.2. Lensing Magnification

Next, we study the statistics of the lensing magnifications. In order to obtain meaningful statistics, and be able to study properties of light rays with a large magnification, which are very rare among random lines of sight, we perform  $10^7$  experiments for each model.

In Figure 5, we plot the probability distributions of image magnifications of a point-like source. For each model, the top panel shows the differential distribution  $p(\mu)$ , and the bottom panel shows the

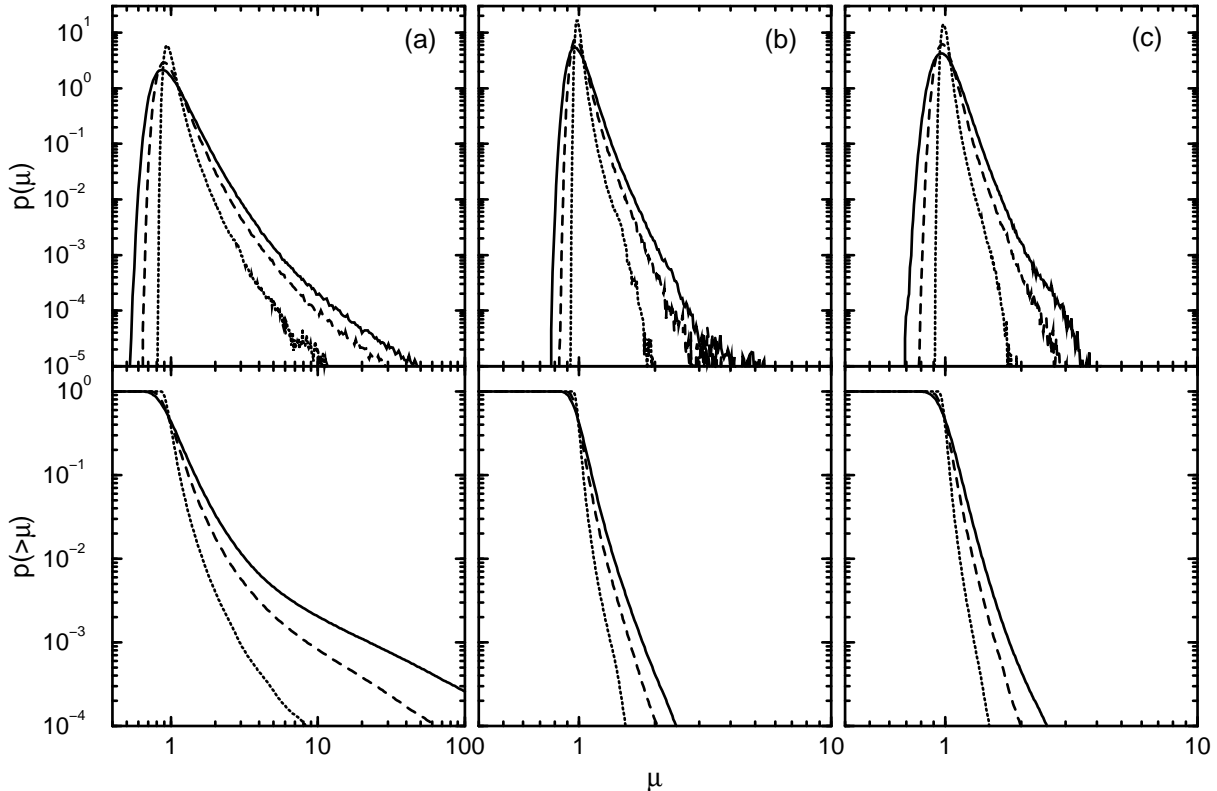


Fig. 5.— Probability distributions of image magnifications. The solid lines are for the source redshift  $z_s = 3$ , dashed lines are for  $z_s = 2$ , and dotted lines are for  $z_s = 1$ . (a) E-dS model; (b) O model; (c)  $\Lambda$  model. For each model, top panel shows the differential distribution  $p(\mu)$ , and bottom panel shows the integral one  $p(> \mu)$ .

integral distribution  $p(> \mu)$ . The probability distributions are normalized so as to satisfy the normalization constraint  $\int_0^\infty d\mu p(\mu) = 1$ . In the differential distributions, we find that the distributions have a strong peak located at values of  $\mu$  slightly less than 1, and are significantly skewed toward large magnifications. In the case of the E-dS model, (Figure 5a), a power-law tail of the form  $p(\mu) \propto \mu^{-2}$  appears at high magnifications, for sources located at redshifts  $z_s = 2$  and 3. This power-law behavior is a general property of the lens equation for a point-like source (see, e.g., SEF, chapter 11). The appearance of this power-law tail indicates the existence of caustics.

The magnification distributions shown in Figure 5 can be interpreted as the “transfer function” of the matter in the universe (Wambsganss et al. 1998). In other words, any intrinsic luminosity function of, say, quasars will be folded with this magnification distribution, and what we measure as the observed quasar luminosity function will be the convolution of the intrinsic luminosity function with this transfer function of the universe (Turner 1980; Avni 1981; Canizares 1982; Peacock 1982; Vietri & Ostriker 1983; Vietri 1985; Ostriker & Vietri 1986; Schneider 1992). Therefore, it is essential to study first the magnification distribution in order to compute the magnification bias accurately. We shall discuss this point in detail in §4.

Since gravitational lensing not only magnify sources but also causes a distortion of their area on the sky, the lines of sight used in our experiments, which are randomly distributed on the *image plane* are not randomly distributed on the *source plane* (Ehlers & Schneider 1986). The small area of a source on the source plane is enlarged by a factor of  $\mu$  on the image plane. Therefore if one averages the lensing magnifications over images randomly distributed on the *image plane*, the resulting average magnification  $\langle\mu\rangle$  will be larger than unity. Taking the effect of area distortion into account, the probability distribution of the lensing magnifications of sources, i.e., the probability distribution calculated from the magnifications of sources randomly distributed on a source plane, is given by

$$p_s(\mu) = \frac{p(\mu)}{\mu}. \quad (19)$$

Notice that, by definition, the mean magnification over sources automatically becomes unity,

$$\langle\mu\rangle = \int_0^\infty d\mu \mu p_s(\mu) = \int_0^\infty d\mu p(\mu) = 1. \quad (20)$$

Using the probability distributions shown in Figure 5, we calculated the dispersions of the magnification distributions,

$$\sigma_\mu^2 = \int_0^\infty d\mu (\mu - 1)^2 p_s(\mu) \simeq \sum_i (\mu_i - 1)^2 p_s(\mu_i), \quad (21)$$

where the probability distribution functions  $p_s(\mu)$  are sampled in bins equally spaced in intervals of 0.01 in  $\log \mu$ , in the range  $0.1 \leq \mu \leq 100$ . The results are shown as filled circles in Figure 6. The solid curves represent the predictions of the power spectrum approach, using the nonlinear power spectrum of Peacock & Dodds (1996), and the dashed curves represent predictions based on the top-hat filtered density field with a smoothing scale of  $R_s = 0.1h^{-1}\text{Mpc}$ . The dispersions in the E-dS model are larger than those in the O and  $\Lambda$  models by about a factor of 3. In all models, the magnification dispersion is larger than 0.1 for a source redshift  $z_s = 3$ . The effect of magnification dispersion on observations of sources will clearly be important for such high redshifts, especially if the density parameter  $\Omega_0$  is large.

Figures 6b and 6c show that, for the O and  $\Lambda$  models, the dispersions obtained from the experiments are in good agreement with the predictions of the nonlinear method, but are larger than the predictions of the *filtered* nonlinear method, as in the cases of lensing convergences and shears. This is again consistent with the trend found in the two-point correlation function at least qualitatively; i.e., the fitting formula of the power spectrum of Peacock & Dodds (1996) underestimates the two-point correlation functions for the O and  $\Lambda$  models. Figure 4a shows that for the E-dS model, the rms values agree with the predictions of the filtered nonlinear method when the source redshift is smaller than 1. However, the growth of  $\sigma_\mu$  with the source redshift is more rapid than the filtered nonlinear method predicts. This rapid growth reflects the appearance of the power-law tail in the magnification distribution. In the power spectrum approach, a perturbative treatment is adopted for calculating the lensing magnification, and thus high magnification events are not properly taken into account. Therefore, the dispersion of lensing magnification estimated from the power spectrum approach should be regarded as a lower limit.

Notice that the integral in equation (21) diverges once the power-law behavior at the high magnification appears. In our calculations, this divergence is prevented by the fact that we have a finite number of experiments: the probability  $p_s$  eventually drops to zero at some value of  $\mu$ , simply because no experiments have produced larger values. In the real universe, the integral does not diverge because the power-law tail

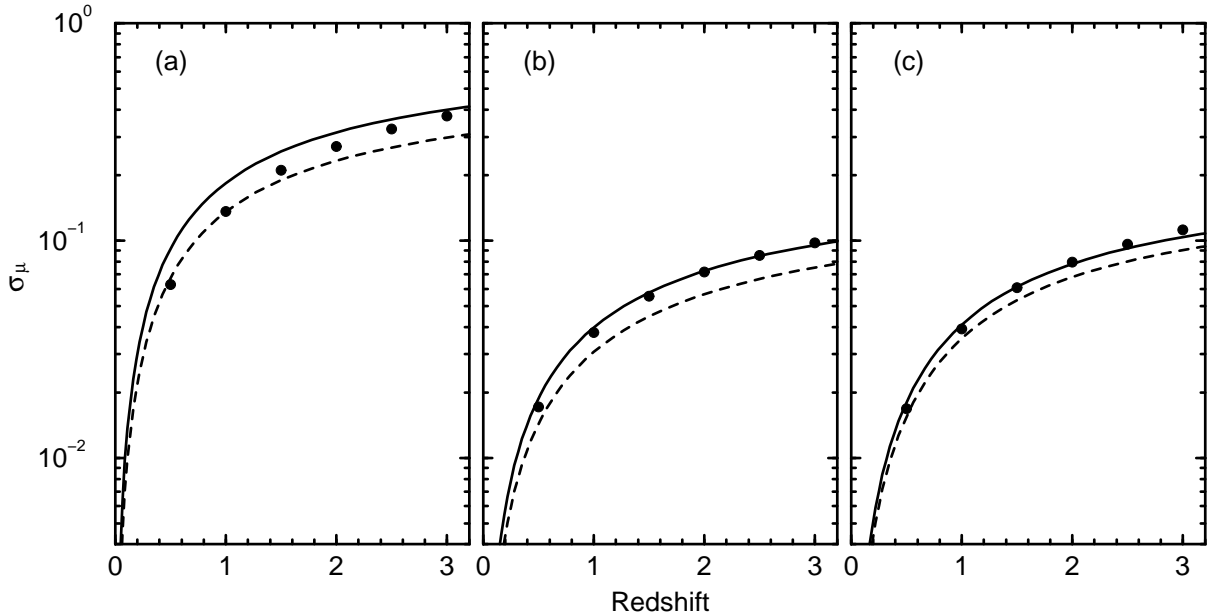


Fig. 6.— The dispersions in the lensing magnification of sources  $\sigma_\mu$  versus source redshift. The filled circles are evaluated from the results of the ray-tracing experiments. The solid curves represent predictions of the nonlinear method, dashed curves are those of the filtered nonlinear method. (a) E-dS model; (b) O model; (c)  $\Lambda$  model.

is effectively cut off at large magnifications. This is caused by the following two effects. First, astrophysical sources are extended, and their magnifications (given by the surface brightness-weighted point-source magnification over the solid-angle area of the source) remain finite (e.g. Bontz 1979; Schneider 1987a; see also SEF, chapter 12). Second, even a point source can only be magnified by a finite value, because the geometrical optics approximation is inadequate near critical curves. A more accurate treatment, based on a wave-optics description of lensing, shows that the magnification is always finite (e.g., Ohanian 1974; 1983; Bliokh & Minakov 1975; Nakamura 1998; also see SEF, chapter 7).

We should note here that, as was mentioned above, the rms values are sensitive to the normalization of the density contrast field,  $\sigma_8$ , i.e. roughly  $\sigma_\mu \propto \sigma_\kappa$ ,  $\sigma_\gamma \propto \sigma_8$  (Bernardeau et al. 1997; Jain & Seljak 1997; Nakamura 1997). Thus the large rms values and the appearance of the power-law tail in magnification distribution in E-dS model are partly due to the high normalization in the model. Observations of the local cluster abundance also place constraints on the value of  $\sigma_8$  which suggest low normalizations  $\sigma_8 \sim 0.5$  to  $0.6$  for the flat model with  $\Omega_0 = 1$  (e.g., Eke, Cole & Frenk 1996; Kitayama & Suto 1996, 1997; Viana & Liddle 1996). The E-dS model might be, therefore, considered as an extreme case.

#### 4. EFFECT OF THE MAGNIFICATION BIAS ON QUASAR LUMINOSITY FUNCTIONS

Strictly speaking, almost all cosmological observations are under the influence of the lensing magnification, but there are very large differences in degree; the majority of field distant sources (say, redshift  $z_s > 1$ ) might be demagnified slightly (Wambsganss et al. 1998), whereas strongly lensed sources such as multiply-imaged quasars and giant luminous arcs, which are relatively very rare, are highly magnified (see e.g. SEF; and for a recent review, Mellier 1999).

In this section, we study the effect of the magnification bias on quasar luminosity functions, using the magnification distributions obtained from the ray-tracing experiments described in §§2 and 3. Although magnification bias is not a phenomenon restricted to quasars alone, we focus our attention on these sources, as previous authors have done (e.g., Schneider 1992), because lensing effects are most relevant to them, due to their inferred compactnesses and large cosmological distances.

We use the conventional definition of the luminosity function  $\Phi(L, z)$  of quasars, as being the comoving number density of quasars at a redshift  $z$  with a luminosity  $L$ . We designate by  $\Phi_{\text{int}}(L, z)$  the *intrinsic luminosity function* of quasars, which is the actual luminosity function, and by  $\Phi_{\text{obs}}(L, z)$  the *observed luminosity function*, which is the luminosity function inferred from observations. Observers compute  $\Phi_{\text{obs}}(L, z)$  by counting sources in redshift bins, and estimating their luminosities from their apparent brightnesses and the luminosity distance  $D_L(z)$  corresponding to each redshift bin. In general,  $\Phi_{\text{obs}}(L, z)$  and  $\Phi_{\text{int}}(L, z)$  differ in presence of gravitational lensing. A source believed to have a luminosity  $L$  might actually be a source with luminosity  $L/\mu$  which is magnified<sup>5</sup> by a factor  $\mu$ . If we neglect any other uncertainty in the determination of  $\Phi_{\text{obs}}$ , then  $\Phi_{\text{obs}}(L, z)$  and  $\Phi_{\text{int}}(L, z)$  are related by

$$\Phi_{\text{obs}}(L, z) = \int_0^\infty d\mu \Phi_{\text{int}}\left(\frac{L}{\mu}, z\right) p_s(\mu, z) \quad (22)$$

(SEF, chapter 12). In the absence of lensing, that is, in a smooth Friedmann universe,  $p_s(\mu, z)$  is equal to a Dirac  $\delta$ -function  $\delta_D(\mu - 1)$ , and equation (22) reduces to  $\Phi_{\text{obs}} = \Phi_{\text{int}}$ . We define the *bias parameter*  $b_Q$  as

$$b_Q \equiv \frac{\Phi_{\text{obs}}(L, z)}{\Phi_{\text{int}}(L, z)}. \quad (23)$$

To compute the magnification bias, we need two ingredients: the magnification probability  $p_s(\mu, z)$  and the intrinsic luminosity function  $\Phi_{\text{int}}(L, z)$ . The former is provided by our ray-tracing experiments. For the latter, we consider two empirical models: a single power-law model, and a double power-law model.

##### 4.1. Single Power-law Model

Let us first consider an intrinsic luminosity function described by a single power-law model,

$$\Phi_{\text{int}}(L, z) = \Phi^*(z) \left(\frac{L}{L^*}\right)^{-\alpha}, \quad (24)$$

---

<sup>5</sup>or demagnified, since  $\mu$  can be either larger or smaller than unity.



where the amplitude  $\Phi^*(z)$  depends on redshift but not luminosity. The power index  $\alpha$  of the luminosity function is uncertain, but is believed to be in the range  $\alpha \sim 1.2 - 1.6$  at the faint end of the luminosity function, and  $\alpha \sim 3 - 4$  at the bright end (Boyle et al. 1988; La Franca & Cristiani 1997). Hence, a single power-law model is not a particularly good approximation for  $\Phi_{\text{int}}$ . However, this model is interesting from a theoretical viewpoint.

We substitute equation (24) in equation (22), and get

$$\Phi_{\text{obs}}(L, z) = \Phi_{\text{int}}(L, z) \int_0^\infty d\mu \mu^\alpha p_s(\mu, z). \quad (25)$$

In this case, the bias parameter is

$$b_Q = \int_0^\infty d\mu \mu^\alpha p_s(\mu, z). \quad (26)$$

Notice that  $b_Q$  is a function of  $z$ , but not  $L$ . Hence, in the case of the single power-law model, the logarithmic slope of the luminosity function is unchanged by the magnification bias, but the amplitude is multiplied by a redshift-dependent factor, and can either increase or decrease, depending on the power index  $\alpha$  and the probability distribution  $p_s(\mu, z)$ . Notice also that in the particular case of a power-law index  $\alpha = 1$ , we get  $\Phi_{\text{obs}} = \Phi_{\text{int}}$ . The observed luminosity functions in a smooth Friedmann universe and in an inhomogeneous Friedmann universe are then equal, in spite of the presence of lensing magnification.

We computed the bias parameter  $b_Q$  as a function of the power-law index  $\alpha$ , using the probability distribution functions derived from our ray-tracing experiments. As in §3.2, we limited the integration range to  $0.1 \leq \mu \leq 100$ . We considered three particular source redshifts,  $z_s = 1$ ,  $z_s = 2$ , and  $z_s = 3$ . The results are plotted in Figure 7. The bias strongly depends on the power index  $\alpha$ . Since the actual quasar luminosity function becomes steeper as the luminosity increases, the effect of magnification bias should be more important at the bright end of the luminosity function than at the faint one. Figures 7b and 7c show that the biasing effect is moderate for the O and  $\Lambda$  models, and is at most 10% even for sources at  $z_s = 3$ . On the other hand, the biasing is considerable for the E-dS model. Even for sources at moderate redshift,  $z_s = 1$ , the bias parameter  $b_Q$  is 4 for  $\alpha = 4$ . For sources at  $z_s = 2$  and 3, the bias parameter strongly grows with  $\alpha$  for the E-dS model. This is mainly due to the presence of the power-law tail in the magnification distributions that we saw in Figure 5a. When the power-law tail appears in the magnification probability, the bias parameter scales roughly as  $b_Q \propto \mu_{\text{max}}^{\alpha-2}$ , where  $\mu_{\text{max}}$  is the upper value of the integration over  $\mu$ , in our case  $\mu_{\text{max}} = 100$ . This implies that the magnification bias diverges in the limit of large magnifications, corresponding to low luminosities, when  $\alpha > 2$ . This divergence is essentially an artifact of the single power-law model used here. The actual luminosity function flattens at the faint end, and the power-law index drops below 2, thus eliminating the divergence. Furthermore, the finite size of the source size becomes an important effect for very highly magnified sources (say  $\mu > 10^3$ , Schneider 1987c, 1992). Schneider & Weiss (1988b) and Schneider (1992) have pointed out that the magnification distribution is effectively cut off like  $p(\mu) \propto (\mu_c/\mu)^6$  for sources with a finite extend, where  $\mu_c$  is a function of the source extend and the mass of a lens. In the case we considered (i.e. distant quasars lensed by large-scale structure),  $\mu_c$  is larger than  $10^3$  (see, e.g., SEF, chapter 12). We do not need to take this effect into account here, because the upper limit of the integration,  $\mu_{\text{max}}$ , is smaller than  $\mu_c$ .

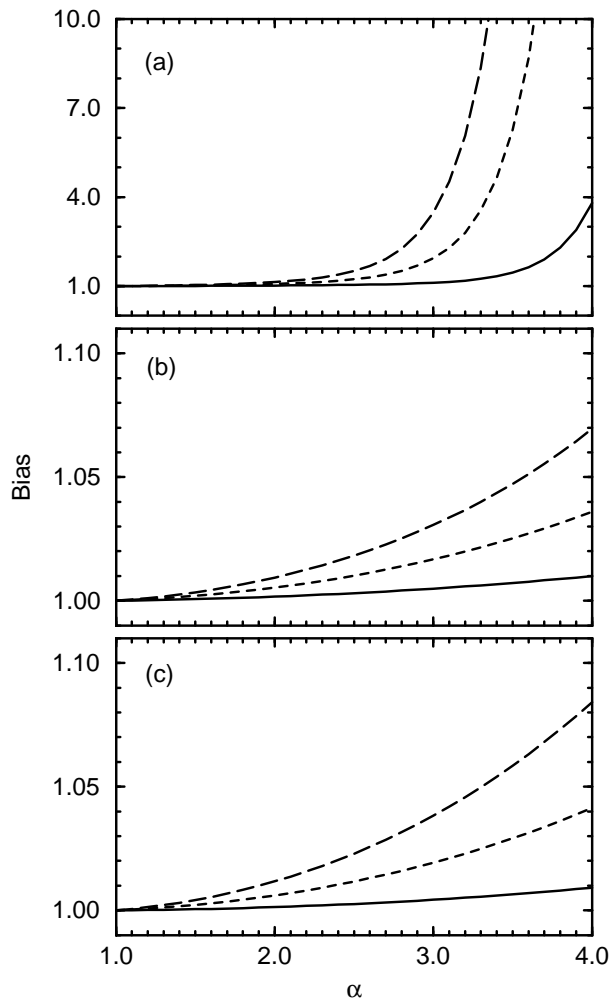


Fig. 7.— The bias parameter  $b_Q$  as a function of a power index  $\alpha$ . The intrinsic luminosity function is taken by the single power-law form, equation (24). The solid lines are for the source redshift  $z_s = 1$ , dashed lines are for  $z_s = 2$ , and long-dashed lines are for  $z_s = 3$ . (a) E-dS model; (b) O model; (c)  $\Lambda$  model.

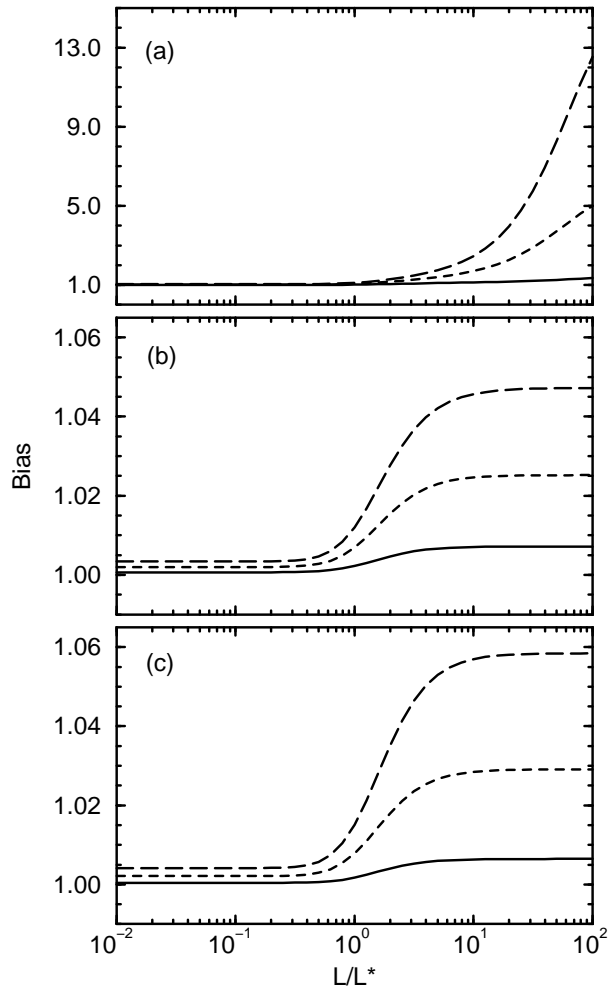


Fig. 8.— The bias parameter  $b_Q$  as a function of a luminosity normalized by its characteristic value,  $L/L^*$ . The intrinsic luminosity function is taken by the double power-law form, equation (27), with  $\alpha_1 = 1.5$ , and  $\alpha_2 = 3.5$ . The meanings of lines are the same as in Figure 7. (a) E-dS model; (b) O model; (c)  $\Lambda$  model.

#### 4.2. Double Power-law Model

Since the power-law index of the luminosity functions appears to take different values at the bright and faint ends, a single power law model, such as the one considered in §4.1, does not provide a very good fit, for any value of the power-law index  $\alpha$ . A much better fit can be obtained by considering a double power-law model of the form

$$\Phi_{\text{int}}(L, z) = \frac{\Phi^*(z)}{(L/L^*)^{\alpha_1} + (L/L^*)^{\alpha_2}}, \quad (27)$$

where  $\alpha_1$  and  $\alpha_2$  are the logarithmic slope of the faint and bright end sides of the luminosity function, respectively. We choose  $\alpha_1 = 1.5$ , and  $\alpha_2 = 3.5$  which are typical values (Boyle et al. 1988; La Franca & Cristiani 1997).

In Figure 8, we plot the biasing parameter  $b_Q$  in units of its characteristic value  $L^*$ . Figures 8b and 8c show that the magnification bias is moderate for O and  $\Lambda$  models. The bias enhances the luminosity functions by about 5% at most at the bright end, and has little effect (below 1%) at the faint end. On the other hand, the effect is significant in the E-dS model, especially for sources at high redshift,  $z_s > 2$ . At the present time, high- $z$  quasars seems to be homogeneously sampled to 2 or 3 magnitude brighter than their characteristic value  $M^*$  (which corresponds to a luminosity  $L \sim 10L^*$ , e.g., La Franca & Cristiani 1997). Figure 8a shows that, for the E-dS model, the bright end of luminosity function (at  $L \sim 10L^*$ ) is enhanced by a factor larger than 2 for such high- $z$  quasars. In this case, the observed luminosity function of bright quasars is strongly biased by the lensing magnification effect.

As an illustrative example, we plot in Figure 9, for the E-dS model, the observed luminosity function as a function of the luminosity in units of its characteristic value  $L^*$ , together with the intrinsic luminosity function, for sources at redshifts  $z_s = 2$  (dashed line) and at  $z_s = 3$  (long-dashed line). The lensing bias flatten the slope of the luminosity functions at the bright end of the luminosity function, above the characteristic luminosity  $L^*$ . If we fit the observed luminosity functions using the same double power-law model (eq. [27]) as for the intrinsic luminosity function, we find that the values of  $L_*$  and  $\alpha_1$  are the same, but the “observed” power-law index  $\alpha_2$  takes the values  $\alpha_{2,\text{obs}} = 3.0$ , and  $\alpha_{2,\text{obs}} = 2.8$  for  $z_s = 2$  and 3, respectively, compared to  $\alpha_2 = 3.5$  for the intrinsic luminosity function. Since the observed power-law index depends on the source redshift, it is essential to take into account the lensing magnification bias when studying the evolution of the *intrinsic* quasar luminosity functions, in order to untangled the effects of magnification bias and genuine luminosity and/or number evolution.

### 5. SUMMARY AND CONCLUSION

We have studied the statistical properties of gravitational lensing by large-scale structure, for three different *COBE*-normalized cosmological models. We used a P<sup>3</sup>M  $N$ -body code to simulate the formation and evolution of large-scale structure, and then used the multiple lens-plane algorithm to follow light rays propagating through the inhomogeneous matter distribution in the universe. For each model, we followed the propagation of  $1.1 \times 10^7$  light rays, from the observer up to a source redshift of 3, and computed the evolution of the Jacobian matrix along each ray. Having such a large number of light rays enabled us to compute, as a function of source redshift, the distributions and rms values of the lensing convergences, shears, and magnifications, to high accuracy. We compared these results with various analytical estimates based on the power spectrum method. Finally, by combining the magnification probability obtained from the experiments with empirical models for the intrinsic luminosity function, of quasars, we computed the

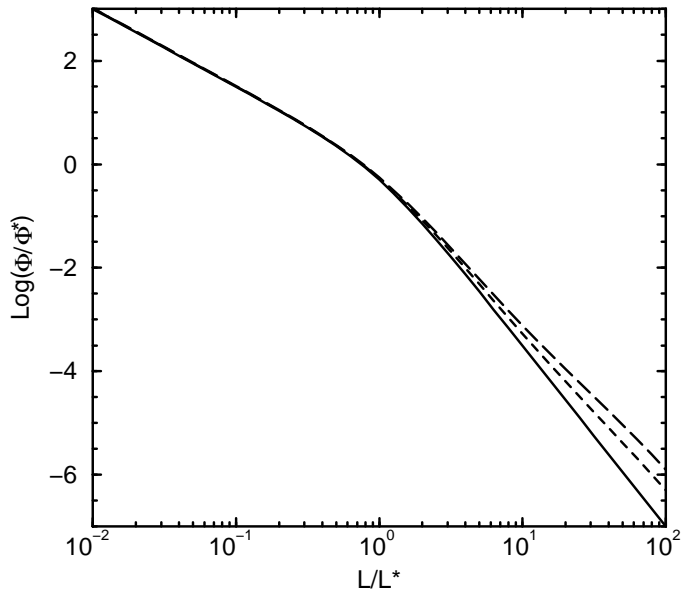


Fig. 9.— The observed luminosity function at the redshifts  $z = 2$  (the dashed line), and  $z = 3$  (the long-dashed line) are plotted as a function of the luminosity normalized by its characteristic value,  $L/L^*$ , together with the intrinsic luminosity function (the solid line). The intrinsic luminosity function is taken by the double power-law form, equation (27) with the power indices  $\alpha_1 = 1.5$ , and  $\alpha_2 = 3.5$ . The background cosmology is taken by E-dS model.

magnification bias. Our main results can be summarized as follows:

1. The rms values of the lensing convergences and shears, which are expected to be equal according to analytical arguments, were found to be nearly equal, the difference being attributed to the finite resolution of the numerical methods used for the simulations. These values were consistent with analytical predictions based on the power spectrum approach with nonlinear evolution of the power spectra.
2. The dispersion of the lensing magnifications strongly depends on the amplitude of the density fluctuations of the matter and thus depends on the density parameter  $\Omega_0$ . The dispersion becomes larger than 0.1 at  $z_s = 1$  for the E-dS model, and at  $z_s = 3$  for the O and  $\Lambda$  models. The magnification distributions are considerably skewed toward high magnification. In particular, a power-law tail appears at large magnifications in the E-dS model, for sources at redshifts  $z_s > 1$ .
3. We have compared the statistics of the lensing magnification with the nonlinear predictions of the power spectrum approach. We found that the power spectrum approach with the nonlinear power spectrum correctly predicts the value of the dispersion of the magnification in the absence of the power-law tail. However, once the power-law tail appears, the predicted values become inaccurate, because the dispersions grow more rapidly with the source redshift than the nonlinear predictions. These predictions, therefore, should be regarded as a lower limit.

4. We studied the magnification bias on quasar luminosity functions. We found that the lensing magnification bias strongly depends on the slope of the luminosity function and on the density parameter  $\Omega_0$ . If the mean matter density is as high as in the E-dS model, the biasing effects can be significant, especially at the bright end of the luminosity function where its slope is very steep. Moreover, since quasar luminosity functions become steeper with the luminosity, the lensing bias will flatten the effective slope of an observed luminosity functions at the bright side.

The power-law tail did not appear in the O and  $\Lambda$  models because the large-scale structure in these models is not as evolved as in the E-dS model. However, the existence of strongly magnified images, such as multiply imaged quasars or galaxies and giant luminous arcs, suggests that whatever the background cosmological model is, there is a power-tail in the actual magnification distribution. Therefore, in order to study the effect of lensing magnification bias on the observed luminosity function, one must carefully take into account the influence of this power-law tail. It is also important to emphasize that, as we have stated in §3.2, the large lensing effects found in the E-dS model are partly due to the high normalization used for that model. Therefore, the E-dS model should be considered as an extreme case.

We have investigated the magnification bias resulting from the gravitational lensing in universes with realistic matter distributions. In order to study quantitatively the biasing effects on the observed quasar luminosity functions, one has to take into account additional selection effects such like the finite extent of a source, which have not been considered in this paper. Such effects will be studied in future works.

We would like to thank P. Premadi for useful discussions. This research was supported in part by the Grants-in-Aid by the Ministry of Education, Science, Sports and Culture of Japan (09640332). HM was supported by NASA Grants NAG5-2785 and NAG5-7363, and a fellowship from the Texas Institute for Computational and Applied Mathematics. The P<sup>3</sup>M simulations were performed at the High Performance Computing Facility, University of Texas.

## A. CALCULATION OF THE VARIANCES

In this Appendix, we present the analytic formulae for calculating the variances of the lensing convergences, shears, and magnifications. Those formulae have been derived by Kaiser (1992, 1998), Villumsen (1996), Bernardeau et al. (1997), Frieman (1997), Jain & Seljak (1997), and Nakamura (1997). We refer the reader to these references for details, and only present the final expressions.

In the weak gravitational field limit, the variance of the lensing convergence and shear can be estimated using both the Born approximation (Schneider et al. 1998) and Limber's equation in Fourier space (Kaiser 1992; 1998). These variance, which turn out to be equal, are related to the density power spectrum, by

$$\sigma_\kappa^2[a(\chi)] = \sigma_\gamma^2[a(\chi)] = \frac{9\Omega_0^2}{8\pi} \left(\frac{H_0}{c}\right)^4 \int_0^\chi dv \left[ \frac{D(0,v)D(v,\chi)}{a(v)D(0,\chi)} \right]^2 I(v), \quad (\text{A1})$$

where  $\chi$  is the *comoving distance*,  $D(\chi_1, \chi_2)$  is the standard angular diameter distance between  $\chi_1$  and  $\chi_2$ , and  $a$  is the Robertson-Walker scale factor normalized to be unity at the present. The relationship between the comoving distance and the redshift  $z$  can be derived from the Friedmann equation (Jain & Seljak 1997):

$$\chi(z) = \frac{c}{H_0} \int_{1/(1+z)}^1 da [\lambda_0 a^4 + (1 - \Omega_0 - \lambda_0) a^2 + \Omega_0 a]^{-1/2}. \quad (\text{A2})$$

The function  $I(v)$  appearing in equation (A1) is an integral over the power spectrum. It is the particular form of that integral that distinguishes the various approximations. In linear theory, this function is given by

$$I(v) = \int_0^\infty dk k P_L[k, a(v)], \quad (\text{A3})$$

where  $P_L$  is the linear power spectrum, which is a function of the wavenumber  $k$  and the scale factor  $a$ , and the dependence of the comoving distance  $v$  enters only through the scale factor. In the nonlinear approximation, we use instead

$$I(v) = \int_0^\infty dk k P_{\text{NL}}[k, a(v)], \quad (\text{A4})$$

where  $P_{\text{NL}}$  is the nonlinear power spectrum, for which Peacock & Dodds (1996) provide a fitting formula. Finally, for the top-hat filtered density field approximation, we use

$$I(v, R_s) = \int_0^\infty dk k P_{\text{NL}}[k, a(v)] \hat{W}_{\text{TH}}^2(k R_s), \quad (\text{A5})$$

where  $\hat{W}_{\text{TH}}(x) \equiv 3(\sin x - x \cos x)/x^3$  is the Fourier transform of the top-hat window function with smoothing scale  $R_s$ . The expression of the variance of the lensing magnifications have been derived by Frieman (1997) and Nakamura (1997), who found that  $\sigma_\mu^2 = 4\sigma_\kappa^2$ .

## REFERENCES

- Avni, Y. 1981, *ApJ*, 248, L95
- Babul, A., & Lee, M. H. 1991, *MNRAS*, 250, 407
- Bardeen, J. M., Bond, J. R., Kaiser, N., & Szalay, A. S. 1986, *ApJ*, 304, 15
- Bartelmann, M., & Schneider, P. 1991, *A&A*, 248, 349
- Bartelmann, M., & Schneider, P. 1992, *A&A*, 259, 413
- Bernardeau, F., van Waerbeke, L., & Mellier Y. 1997, *A&A*, 322, 1
- Blandford, R. D., & Narayan, R. 1986, *ApJ*, 310, 568
- Bliokh, P. V., & Minakov, A. A. 1975, *Astrophys. Space Sci.*, 34, L7
- Bontz, R. J. 1979, *ApJ*, 233, 402
- Boyle, B. J., & Shanks, T., & Peterson, B. A. 1988, *MNRAS*, 235, 935
- Bunn, E. F., & White, M. 1997, *ApJ*, 480, 6
- Canizares, C. R. 1982, *ApJ*, 263, 508
- Dyer, C. C., & Roeder, R. C. 1972, *ApJ*, 174, L115
- Dyer, C. C., & Roeder, R. C. 1973, *ApJ*, 180, L31

- Ehlers, J., & Schneider P. 1986, *A&A*, 168, 57
- Eke, V. R., Cole, S., & Frenk, C. S. 1996, *MNRAS*, 282, 263
- Frieman, J. A. 1997, *Comments Astrophys.*, 18, 323
- Fukugita, M., Futamase, T., Kasai, M., & Turner, E. L. 1992, *ApJ*, 393, 3
- Futamase, T., & Sasaki, M. 1989, *Phys. Rev. D*, 40, 2502
- Gunn, J. E. 1967, *ApJ*, 150, 737
- Hamana, T. 1998, *Prog. Theor. Phys.* 99, 1085
- Hartwick, F. D. A., & Schade, D. 1990, *ARA&A*, 28, 437
- Hawkins, M. R. S., & Véron, P. 1995, *MNRAS*, 275, 1102
- Hockney, R. W., & Eastwood, J. W. 1988, *Computer Simulation Using Particles* (Bristol: Adam Hilger)
- Hu, W., & Sugiyama, N. 1996, *ApJ*, 471, 542
- Jain, B., & Seljak, U. 1997, *ApJ*, 484, 560
- Jaroszynski, M. 1991, *MNRAS*, 249, 430
- Jaroszynski, M. 1992, *MNRAS*, 255, 655
- Jaroszynski, M., Park, C., Paczynski, B., & Gott, J. R. 1990, *ApJ*, 365, 22
- Kaiser, N. 1992, *ApJ*, 388, 272
- Kaiser, N. 1998, *ApJ*, 498, 26
- Kitayama, T., & Suto, Y. 1996, *ApJ*, 469, 480
- Kitayama, T., & Suto, Y. 1997, *ApJ*, 490, 557
- Kovner, I. 1987, *ApJ*, 316, 52
- Kristian, J., & Sachs, R. K. 1966, *ApJ*, 143, 379
- La Franca, F., & Cristiani, S. 1997, *AJ*, 113, 1517
- Martel, H. 1991, *ApJ*, 366, 353
- Martel, H., & Matzner, R. 1999, submitted to *ApJ*
- Martel, H., Premadi, P., & Matzner, R. 1998, *ApJ*, 497, 512
- Mellier, Y., 1999, *ARA&A*, 37, in press (astro-ph/9812172)
- Nakamura, T. T. 1997, *Publ. Astron. Soc. Japan*, 49, 151
- Nakamura, T. T. 1998, *Phys. Rev. Lett.*, 80, 1138
- Ohanian, H. C. 1974, *Int. J. Theoret.*, 9, 171

- Ohanian, H. C. 1983, *ApJ*, 271, 551
- Ostriker, J. P., & Vietri, M. 1986, *ApJ*, 300, 68
- Peacock, J. A. 1982, *MNRAS*, 199, 987
- Peacock, J. A., & Dodds, S. J. 1996, *MNRAS*, 280, L19
- Peebles, P. J. E. 1993, *Principles of Physical Cosmology* (Princeton: Princeton Univ. Press)
- Premadi, P., Martel, H., & Matzner, R. 1998, *ApJ*, 493, 10
- Premadi, P., Martel, H., & Matzner, R. 1999, in preparation
- Sanitt, N. 1971, *Nature*, 234, 199
- Schneider, P. 1987a, *A&A*, 179, 71
- Schneider, P. 1987b, *A&A*, 183, 189
- Schneider, P. 1987c, *ApJ*, 316, L7
- Schneider, P. 1992, *A&A*, 254, 14
- Schneider, P., Ehlers, J., & Falco, C. C. 1992, *Gravitational Lenses* (Berlin: Springer) (SEF)
- Schneider, P., van Waerbeke, L., Jain, B., & Kruse, G. 1998, *MNRAS*, 296, 873
- Schneider, P., & Weiss, A. 1988a, *ApJ*, 327, 526
- Schneider, P., & Weiss, A. 1988b, *ApJ*, 330, 1
- Tomita, K. 1998a, *Prog. Theor. Phys.*, 99, 97
- Tomita, K. 1998b, *Prog. Theor. Phys.*, 100, 79
- Turner, E. L. 1980, *ApJ*, 242, L135
- Viana, P. P., & Liddle, A. R. 1996, *MNRAS*, 281, 323
- Vietri, M. 1985, *ApJ*, 293, 343
- Vietri, M., & Ostriker, J. P. 1983, *ApJ*, 267, 488
- Villumsen, J. V. 1996, *MNRAS*, 281, 369
- Wambsganss, J., Cen, R., Ostriker, J. P., & Turner, E. L. 1995, *Science*, 268, 274
- Wambsganss, J., Cen, R., Xu, G., & Ostriker, J. P. 1997, *ApJ*, 475, L81
- Wambsganss, J., Cen, R., & Ostriker, J. P. 1998, *ApJ*, 494, 29
- Warren, S. J., & Hewett, P. C., & Osmer, P. S. 1994, *ApJ*, 421, 412
- Weinberg, S. 1972, *Gravitation and Cosmology* (New York: Wiley)